Quantum chemical and molecular dynamics studies of MUC-1 calix[4,8]arene scaffold based anti-cancer vaccine candidates

Angelo Spadaro[1*], Livia Basile[1], Matteo Pappalardo[1*], Carmela Bonaccorso[2], Marco Rao[1], Simone Ronsisvalle[1], Giuseppe Granata[3] and Salvatore Guccione[1*]

[1]Department of Drug Sciences, University of Catania, Viale A. Doria 6, I-95125 Catania, Italy.
[2]Department of Chemical Sciences, University of Catania, Viale A. Doria 6, I-95125 Catania, Italy.
[3] Institute of Biomolecular Chemistry, C.N.R., Via P. Gaifami 18, I-95126 Catania, Italy

Dedicated to the memory of Maria S. Pappalardo

Abstract

Functional antitumor vaccine constructs are the basis for active tumor immunotherapy, which is useful in the treatment of many types of cancers. MUC1 is one key protein for targeting and designing new strategies for multi-component vaccines. Two self-adjuvant tetravalent vaccine candidates were prepared by clustering four or eight PDTRP MUC1 core epitope sequences on calixarene scaffolds. In this work, the different activities of two molecules with calix[4]arene and calix[8]arene skeleton are rationalized. Quantum-Mechanics, Docking and Molecular Dynamics structural optimization were firstly carried out followed by Metadynamics to calculate the energy profiles. Further insights were obtained by molecular fields' complementarity studies. The molecular modelling results are in strong agreement with the experimental *in vivo* immunogenicity data. In conclusion, the overall data shows that in the designing of anticancer vaccines, the scaffold flexibility has a pivotal role in obtaining a suitable electrostatic, hydrophobic and steric complementarity with the biological target.

Keywords: calix[4,8]arene, Molecular Dynamics, Quantum Chemistry, MUC1, Anticancer vaccine

Introduction

The goal of active antitumor immunotherapy is to elicit specific and selective production of antibodies against tumor cells via different approaches, such as through the use of engineered anticancer vaccine constructs.[1, 2] The potential of antitumor immunotherapy is undeniable since it could ensure a robust and durable response that would allow the treatment of different types of cancer even during an advanced stage of the disease.[3, 4]

MUC1 is a highly *O*-glycosylated transmembrane protein typically expressed at the apical surface of normal epithelial cells. In the cancer-associate state, it turns into an autoantigen and its use as a potential target in the development of vaccines for active tumor immunotherapy[5] is very challenging. Overexpression of MUC1 is implicated with cancer cells' invasiveness, metastasis, and resistance to death caused by reactive oxygen species.[6] The MUC1 extracellular domain is composed by tandem repeat sequences formed by 20 amino acids $(GVTSAPDTRPAPGSTAPPAH)_n$ where n varies in the range 30-100 and, as a consequence, the MUC1 extracellular domain may protrude 150−500 nm above the cell membrane.[6]

The extracellular domain of normal MUC1 has a dense cover of highly branched carbohydrates with complex structures. Each mucin tandem repeat sequence contains five potential *O*-glycosylation sites, corresponding to serine and threonine. Moreover, the glycosylation position may change according to the type of tissue.[7] In the neoplastic transformation, MUC1 becomes an autoantigen as a result of incomplete glycosylation processes. This underglycosylation determines the exposure of the "naked" peptide core, such as the highly immunogenic PDTRP sequence, as well as the formation of normally cryptic tumor-associated carbohydrate antigens (i.e., Tn, STn, TF, etc.).[5-7] Therefore, incomplete glycosylation in cancer cells leads to the exposure of epitopes, which are hidden in normal cells.[7]

Cellular and humoral immune responses *versus* MUC1 have been demonstrated in cancer patients. The presence of antibodies against MUC1 in breast tumor patients has been correlated with

a favourable disease outcome. This feature makes tumor-associated MUC1 an interesting target for cancer immunotherapy.[7, 8]

Studies on mice using monoclonal antibodies have demonstrated that the PDTRP sequence is an immunodominant B-cell epitope. In addition, MUC1-expressing tumors of breast cancer patients can elicit both humoral and cellular responses against the PDTRP sequence.[9]

Moreover, the combined approach of an immunostimulant with MUC1 glycopeptides has proved to be very useful in activating the T-cell dependent pathway. Potential immunostimulants are carrier proteins, T-cell epitope peptides, or Toll-like-receptor ligands based on immunologically active lipopeptides. Different combinations of these components have been used to prepare multicomponent vaccines.[7, 8]

Two self-adjuvant multivalent vaccine candidates obtained by assembling four or eight PDTRP MUC1 core sequences on calix[4]arene (calix[4]) and calix[8]arene (calix[8]) skeletons were previously reported by us (Figure 1).[10] To enforce the humoral immune response, the known Toll-like receptor 2 (TLR2) immunoadjuvant tripalmitoyl-*S*-glyceryl-cysteinylserine (P_3CS) was also added to the above-mentioned constructs.[10,11] ELISA assay showed that these constructs stimulated specific anti-MUC1 IgG antibody production with a multivalency effect [10,12, 13] and that the elicited antibodies are capable of recognizing the MUC1 epitopes present on MCF7 human breast cancer cells.[10]

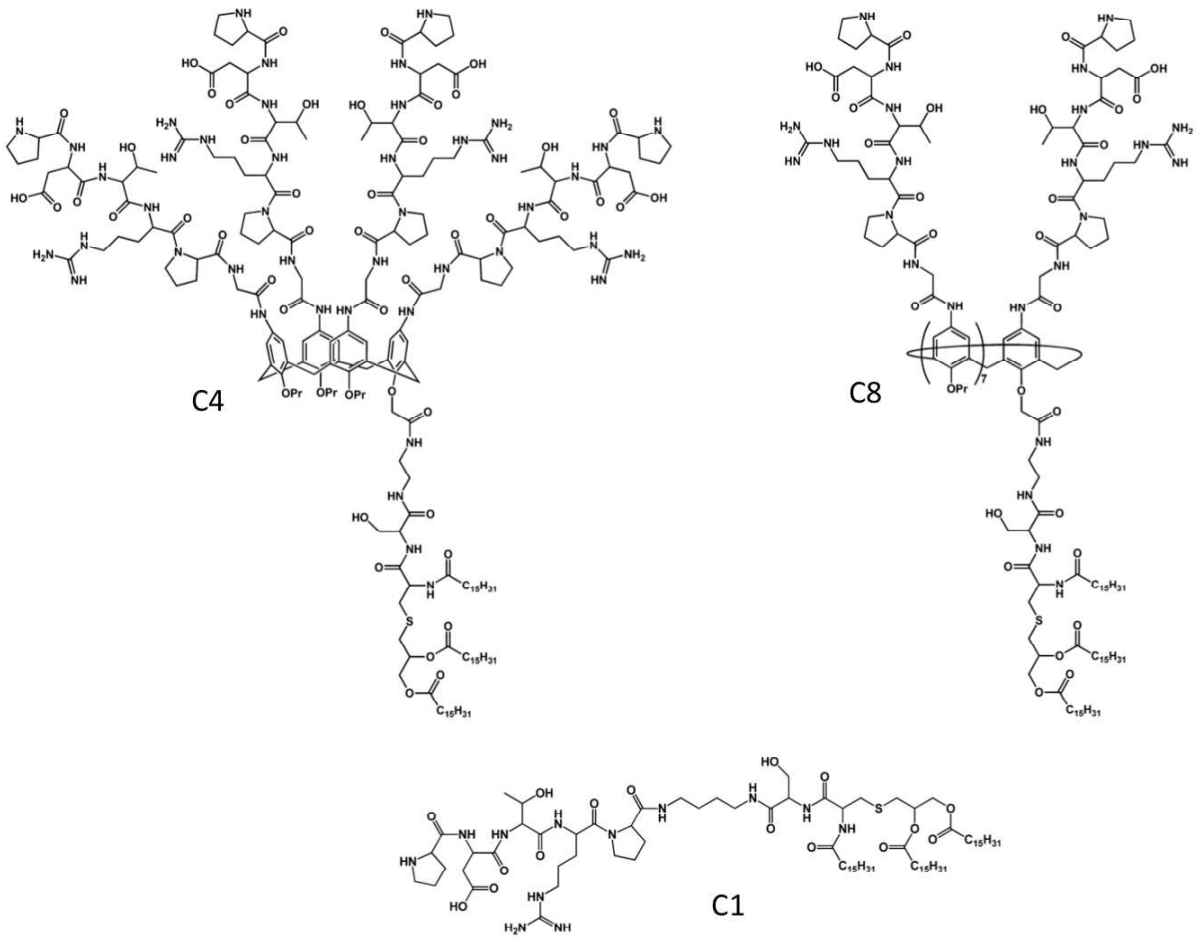

Figure 1: Structure of PDTRP based constructs: calix[4], calix[8] and monovalent reference compound (C1). The PDTRP units were covalently linked to the calixarene upper rim, whereas the P_3CS unit was bounded at the lower rim of the macrocycle. Adapted, with permission, from Spadaro *et al.*[10](Geraci, C.; Consoli, G. M.; Granata, G.; Galante, E.; Palmigiano, A.; Pappalardo, M.; Di Puma, S. D.; Spadaro, A., First self-adjuvant multicomponent potential vaccine candidates by tethering of four or eight MUC1 antigenic immunodominant PDTRP units on a calixarene platform: synthesis and biological evaluation. Bioconjug Chem 2013, 24, 1710-20).

To advance the design of MUC1 vaccines, it is crucial to understand the complex conformational equilibrium of the tumour-associated mucins in both free and bound states. Although the design of glycopeptide vaccines is based on NMR, X-ray and molecular modelling studies performed over the last 15–20 years, there is still much to be learned about the factors that govern antigen presentation and the structural elements required to achieve optimal antigen–antibody interactions.[7] Hybrid

Quantum-Chemical-Molecular Dynamics[14] and Metadynanics[15] were also successfully applied to investigate bioactive conformations and binding determinants of "nonpeptidic" calix[4,8]arene. Studying the correlation between conformational multiplicity, tridimensional architecture, and biological activity of calix[4][16] and calix[8][17] can significantly contribute to the development of new anti-cancer vaccines that are expected to perform more effectively.

Results and discussion

Metadynamics was carried out by only taking into consideration the calix ring to better evaluate its conformational changes during 100 ns of simulation. Only minima obtained from metadynamics simulations were considered.

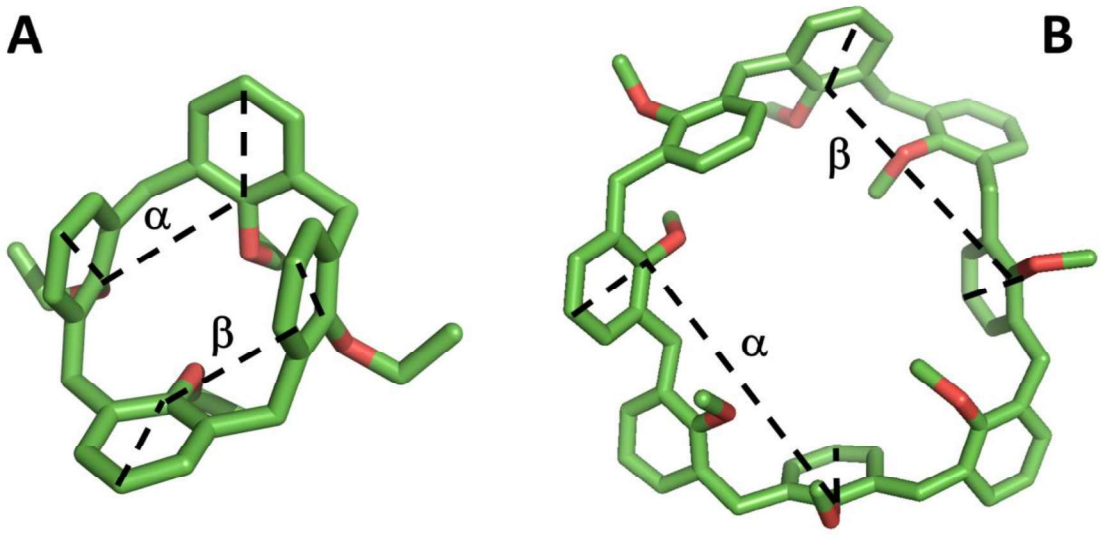

Figure 2: Dihedral angles of the central calixarenic macrocycles of calix[4] (panel A) and calix[8] (panel B) considered for metadynamics simulations.

The dihedral angle variables considered in this study are shown in Figure 2. Dihedral angle variables were selected considering the aromatic rings of the calixarenes macrocycles which are directly connected to the pendant chains, therefore any alterations in the calixarene scaffolds will affect the pendant epitope structures and vice-versa. To identify the best *coval* (collective variables)

some preliminary simulations including ring or chains *end-to-end* distance were performed till the appropriate dihedral angle values were reached. A free energy profile was calculated for both "α and β" dihedral angles variables (Figure 2) of the central calix macrocycle of calix[4] and calix[8] constructs. Minimum energy profiles for calix[4] (Figure 3, panel A) here reported evidenced a small area with a minimum of free energy at α = 37° β = -22.5°. Although the calix[4] structure is symmetrical, the asymmetry in the orange and cyan area of the graph (Figure 3 A) can be caused by conformational fluctuations which reflect in the energy due to the presence of the immunoadjuvant P3CS (N-palmitoyl-S-[2,3-bis(palmitoyloxy)-(2R,S)-propyl]-(R)-cysteinyl-serine) and interactions with the solvent. Both the *partial* and *full cone* conformations of calix[8] (Figure 3, panel B and C, respectively) converge to the same minimum of energy (α = 20° β= -112°) even if the simulations start from different geometries, as below reported. This latter *minimum* value was considered for further analysis by the software Flare 2.0.1 and 3.0[18, 19].

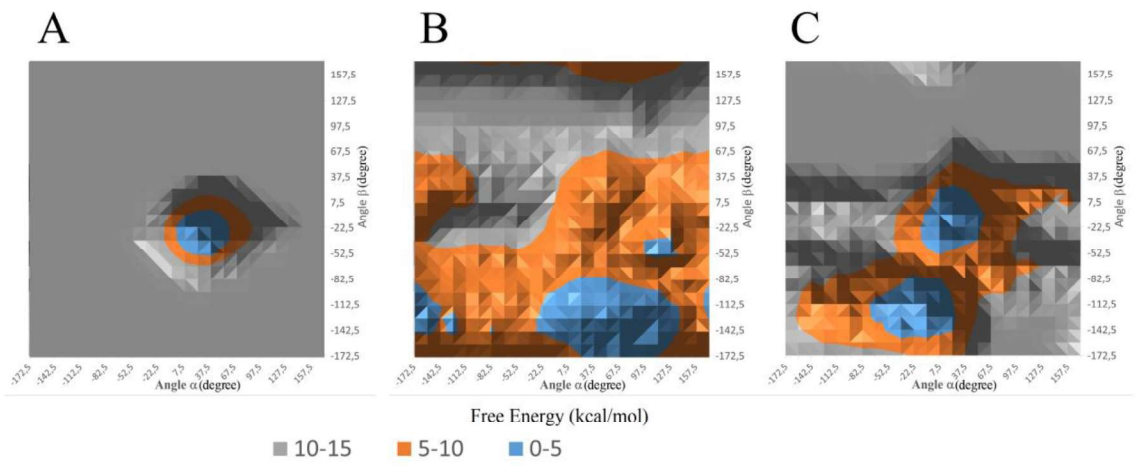

Figure 3: Free energy profile for calix[4] (panel A), and for *partial* and *full cone* conformations of calix[8] (panel B and C, respectively).

MD simulations at the free energy minimum showed that both *full* and *partial cone* geometries of the central calixarenic ring of the calix[8] construct evolve to a common conformation (Figure 4, panel C).

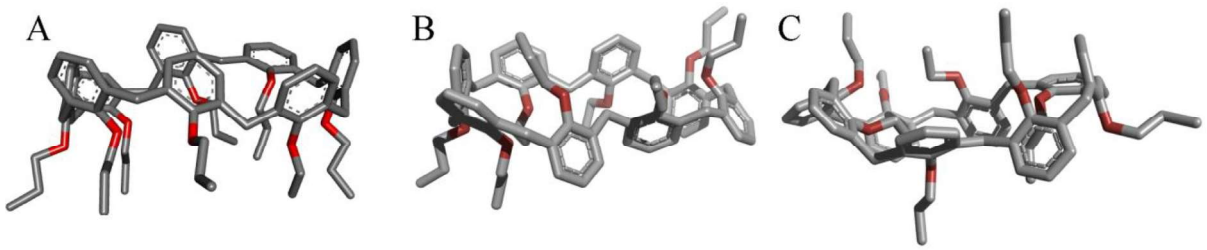

Figure 4: Starting calix[8] structures in a *full cone* (Panel A), *partial cone* (Panel B), conformations and free energy minimum structure (panel C).

The conformation of calix[4] with the hydrophobic areas of the molecule as blue surfaces is shown in Figure 5 (panel A) . The upper and lower rim pendant chains of the calix[4] fold in a *globular-like* structure that looks like a large spherical hydrophobic tail. The calixarene macrocycle is fully exposed to the solvent, bearing pendant chains which include PDTRP moieties at the upper rim along with a P_3CS unit and propoxy groups at the lower rim of the calix cycle (Figure 5).

The calix interaction cavity is flanked by four oxygens as shown in Figure 5

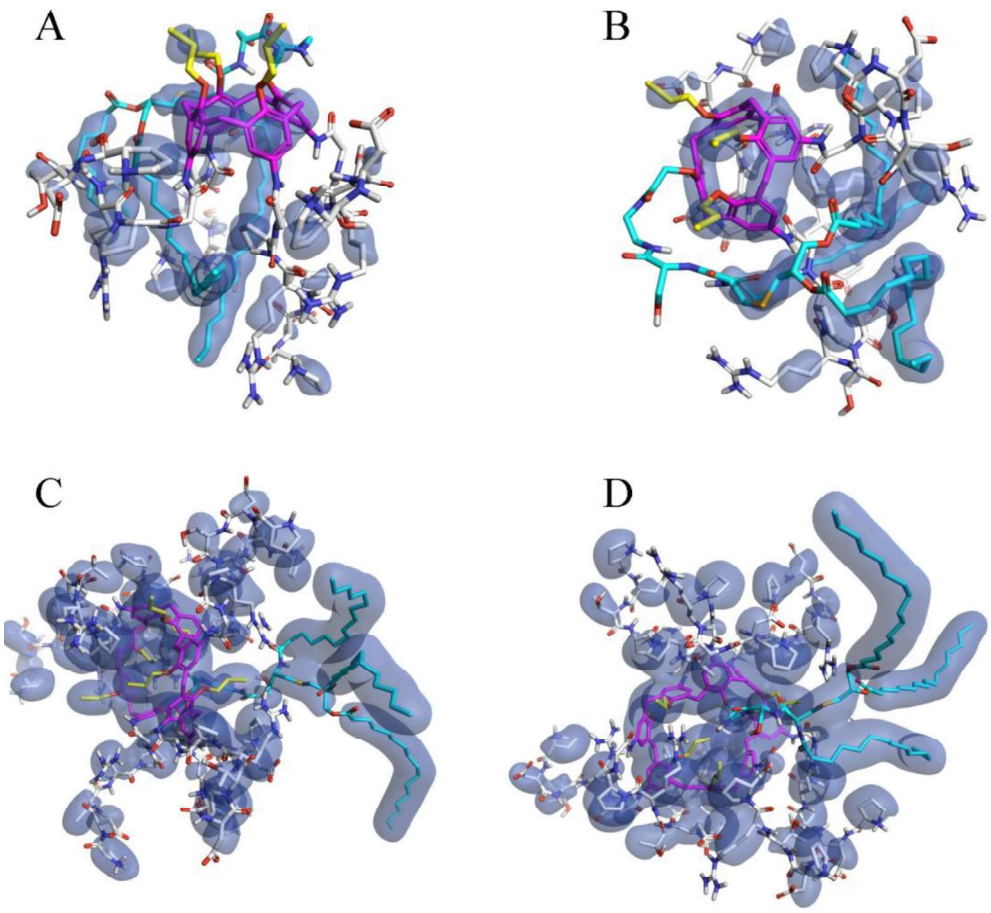

Figure 5: side and top view (panel A and panel B) of calix[4] and calix[8] (panel C and panel D). Calix moiety is in magenta with lower and upper rim pendant chains. Propoxy group and P_3CS moiety are displayed in yellow and cyan sticks, respectively; PDTRP moieties are represented as white sticks. Hydrophobic areas are displayed as blue surfaces.

The minimum energy structure of calix[4] and calix[8] was docked into SM3. This docking was carried out using a simplified model of the calix molecules necessitated by their very high flexibility.

Assuming the calix models were at a minimum of energy only the backbone carbon atoms were allowed to freely move and the relevant torsion angles were considered. All other torsion angles were held fixed. Higher scores were obtained for calix[8] (-25.6 kcal/mol) in respect to calix[4] (18.2 kcal/mol).

Analysis of the SM3 complex with the epitope structure as in the PDB file (pdb code: 1sm3) shows two possible H-bonds with Gln97, Trp 33, and some atomic clashes because of Tyr 32, Trp96, Asn31, Pro56, Val95, and Tyr102. Tyr32 might partially compensate the steric penalty by establishing a H-bond with the epitope. Overall both calix[4] and calix[8] show a common interaction pattern with Asn31, Trp 33, and Tyr32 (Figure 6). Electrostatic complementarity maps of calix in respect to MUC1 and single calix electrostatic maps have been calculated by the software Flare 2.0.1 and 3.0[18, 19] and are discussed below.

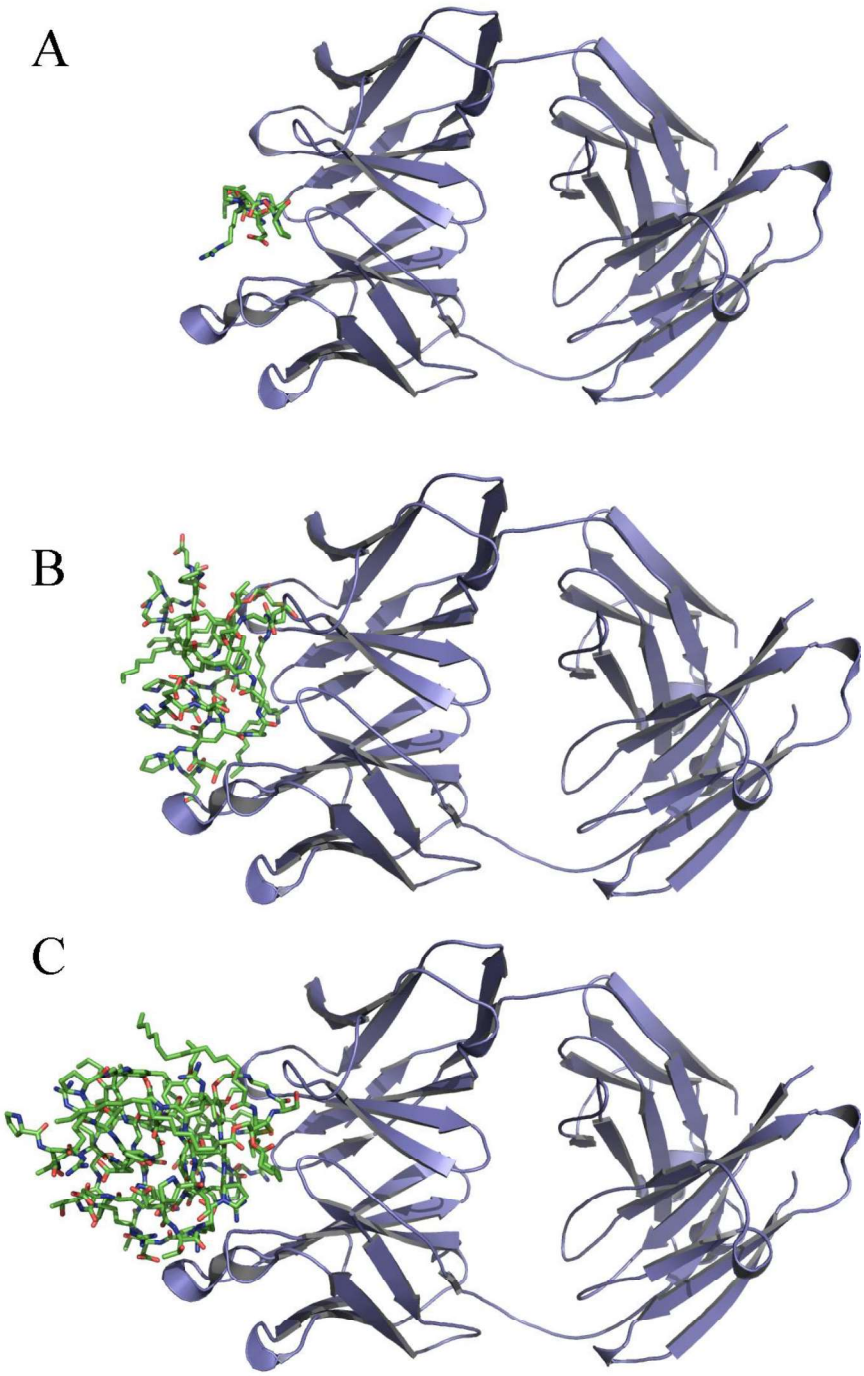

Figure 6: Docking of the free energy minimum structure of calix[4] (panel B), and calix[8] (panel C) with the tumor-specific antibody SM3 (pdb code: 1sm3), and its peptide epitope as reference (panel A).

Analysis of the electrostatic potential could provide useful knowledge on the fundamental processes that underlie bio-molecular binding[20]. These maps of potential hydrogen bonds/hydrogen bonds networks and electron-rich or electron-poor regions around the structures are crucial for molecular recognition and affect the binding free energy.[21]

The analysis of electrostatic maps of calix[4] (Figure 7), showed that both positive (blue) and negative (red) fields are clearly separated and alternatively distributed without discontinuity in the exterior surface of the calix[4] construct which adopts a globular shape.

A completely different behaviour was evidenced for calix[8], which has a huge amount of extended accessible conformers. For this reason, a *partial cone* conformation and a *full cone* conformation of the central calix ring were used, as reported in Figure 4.

With regard to the SM3 antibody, the -NH groups (H-bond donor) of Asn31 and Trp33 (chain H) create a region of positive charges (blue) on the antibody SM3 structure that extends to both the -NH (H-bond donor) of Arg52 (chain H) up and the NH (H-bond donor) of Gln97 (chain H) down.

This positive region (blue) perfectly matches the negative cloud (red) formed by the H-bond acceptor carboxyl of Asp5 and the H-bond acceptor carbonyl of Thr6 of the co-crystallized MUC-1/sm3 complex. Moreover, two negative clouds (red) as defined by three H-bond acceptors –C=O of Tyr32 , Asn31 (chain H) and the –OH group of Tyr32 (chain L) interact with two positive regions (blue) provided by the peptide H-bond donor -NH of Pro10, Ala9 and Pro4(Figure 7, panel C). A detailed description of each residue of calix[4]/calix[8] interacting with SM3 is really difficult since the structure is constituted of repetitive units. Therefore only some more significant areas were identified in accordance with the electrostatic potential maps, as below reported.

Electrostatic maps (Figure 8) of the calix[8] construct reveal that positive (blue) and negative (red) fields extend to the exterior of the molecule and regularly alternate each other showing more mixed up positive and negative charges on the surface, compared to calix[4].

Moreover about eight (8) negative areas with a single positive wide area were detected in the electrostatic potential maps of calix[8]. Electrostatic maps (Figure 8) of the calix[8] construct reveal

that positive (blue) and negative (red) fields extend to the exterior of the molecule and regularly alternate each other showing more mixed up positive and negative charges on the surface. About 19 negative areas and 6-7 positive wide areas were detected. However, the detected pattern alternating negative (red) and positive areas (blue) in the anti-MUC-1 antibody is better reproduced, in both magnitude and number, in the calix[8] surface than that of calix[4]. Hence, it should be supposed that in calix[8] the PDTRP chains assume as a whole a conformation that better fits the binding site of the antibody in terms of the 3D shape.

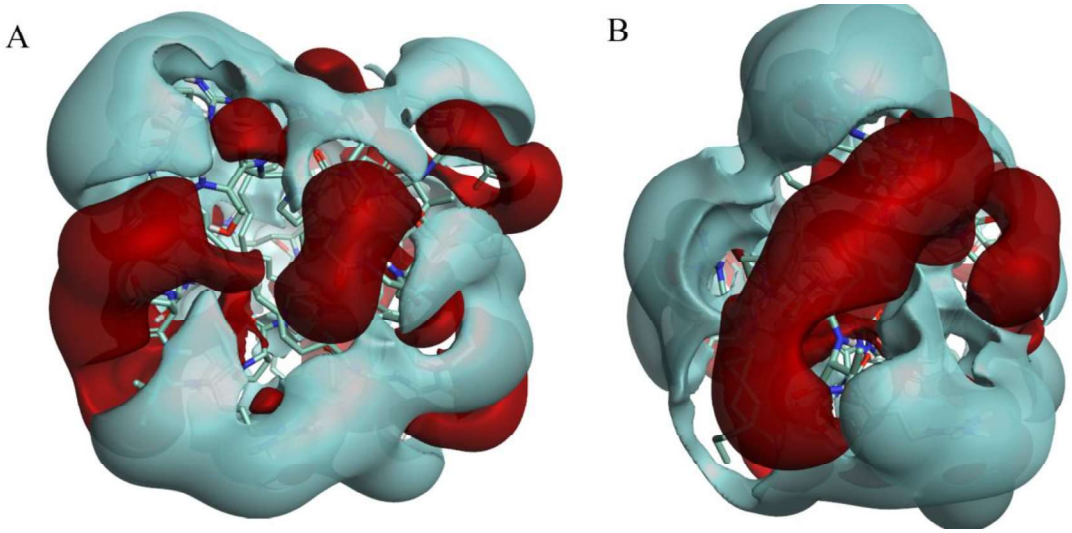

Figure 7: Electrostatic map of calix[4]. Front (A) and back (B) view fields showing electron negative (red) and positive (blue) areas.

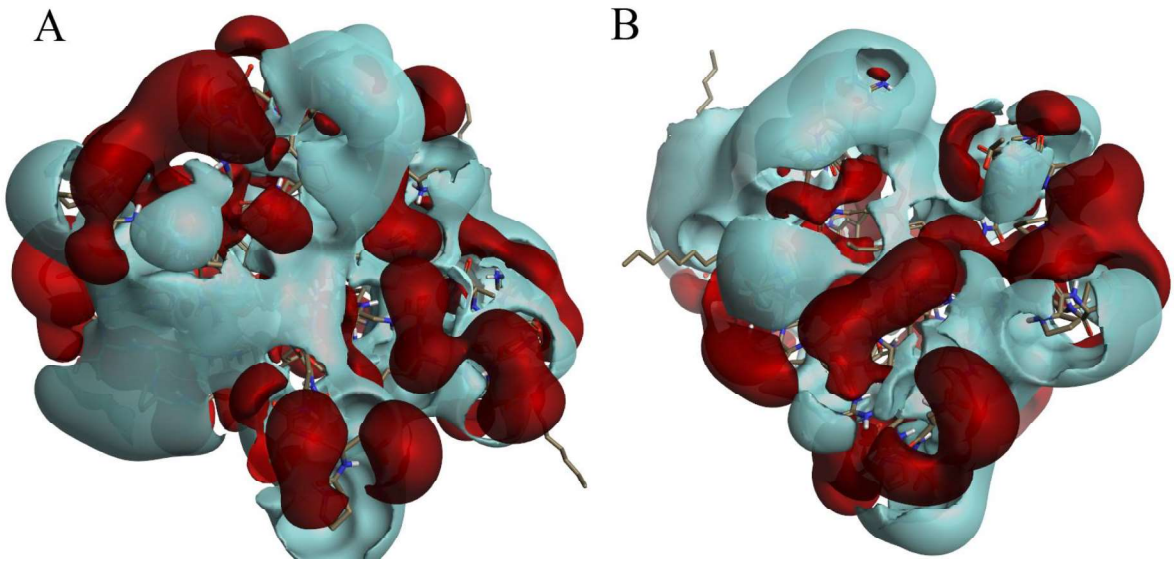

Figure 8: Electrostatic maps of *partial cone* (A) and *full cone* (B) calix[8] conformations. Positive and negative Electron are shown. Electron positive and negative are shown.

The electrostatic profile of the antibody SM3 at the level of the MUC-1 peptide binding site (Figure 9) might be determinant for the binding. As expected, the positive areas of the antibody SM3 match with the negative ones of the MUC-1 and vice versa.. EC map of calix[4] reveals overall a good match with Sm3 (score is 0.051). However a pronounced electrostatic clash occurs between the positive electrostatic potential generated by the amine groups of residues: Gly94, (-NH side-chain and backbone), Asn35 (-NH side chain), Gly 96 (-NH backbone), Gly97 (-NH backbone and sidechain) that overlap the one provided by the -NH groups of calix[4] facing these residues. A better complementarity was found in the case of calix[8] (EC score is 0.089) which shows a more extended green area (perfect electrostatic complementarity). Nevertheless, in the binding cavity Asn31 generates a negative (C=O) and positive (NH) potential that clashes respectively with a positive and negative area of calix[8].

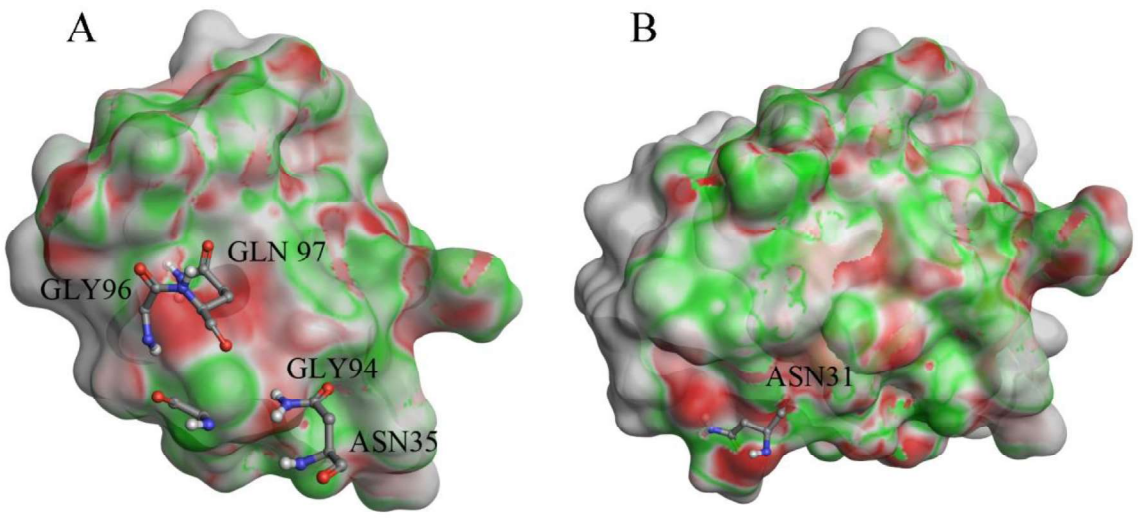

Figure 9: Panel A: Electrostatic complementarity (EC) of calix[4] with SM3. Panel B: Electrostatic complementarity map of calix[8] with SM3**.** Green surface indicates perfect electrostatic complementarity, white surface indicates zero electrostatic potential for both ligand and protein, red surface indicates strong electrostatic repulsion.

The molecular modelling results agree with the experimental immunogenicity data by administration in Balb/c mice of the multiepitopic calixarene constructs (Table 1).

Table 1. End Point Titers after immunization of mice* with calix[4], calix[8] and monovalent reference construct C1.

Construct	IgG Anti-PDTRP
calix[8]	5120
calix[4] (2x)	2560
calix[4] (1x)	1280

All comparisons were significant (two samples rank test) ($p<0.05$). *n=6. Adapted, with permission, from Spadaro et al.[10](Geraci, C.; Consoli, G. M.; Granata, G.; Galante, E.; Palmigiano, A.; Pappalardo, M.; Di Puma, S. D.; Spadaro, A., First self-adjuvant multicomponent potential vaccine candidates by tethering of four or eight MUC1 antigenic immunodominant PDTRP units on a calixarene platform: synthesis and biological evaluation. Bioconjug Chem 2013, 24, 1710-20).

Data obtained from our previous studies[10] showed that mice treated with the same molar quantity of calix[4], calix[8] or the reference monovalent construct C1 elicited the development of specific anti-PDTRP IgG antibodies in the following order of potency calix[8]>calix[4]>C1. Furthermore, a significant multivalent effect was detected for both calixarenic derivatives as opposed to the monovalent C1 construct.[10]

To investigate solutions with the same number of PDTRP epitopes, in order to exclude a concentration effect between the calix[8] and calix[4] constructs, the tetrameric vaccine calix[4] was tested at a double (2x) molar concentration (0.60 μM/mouse) compared to calix[8] (0.30 μM/mouse). An inspection of the reported data (Table 1) reveals that the octameric derivative calix[8] showed a higher antibody response even when the tetrameric derivative calix[4] was tested at a double molar concentration (2x), with a 2-fold higher and statistically significative antibody production. We speculated that we can attribute the higher activity of calix[8] construct to its intrinsic molecular structural characteristics and not to a double number of PDTRP units.

Importantly, the antisera obtained in this study from calix[4] construct tested at (2x) molar concentration (0.60 μM/mouse), similarly to that obtained in our previous studies,[10] showed a good and significative recognition ($p < 0.05$ vs construct C1) of the native MUC1 epitopes expressed on MCF7 human breast cancer cells (Figure 10). Therefore, the array of PDTRP antigens assembled on the calixarene scaffolds represents a good mimicking of the natural MUC1 antigen pattern found *in vivo*.

Put together this data suggests that the higher conformational freedom of the calix[8] vaccine construct could allow for an improved three-dimensional organization of the PDTRP antigens sequences that, in turn, permits more efficient supramolecular adaptive interaction with the Major Histocompatibility Complex (MHC) apparatus.

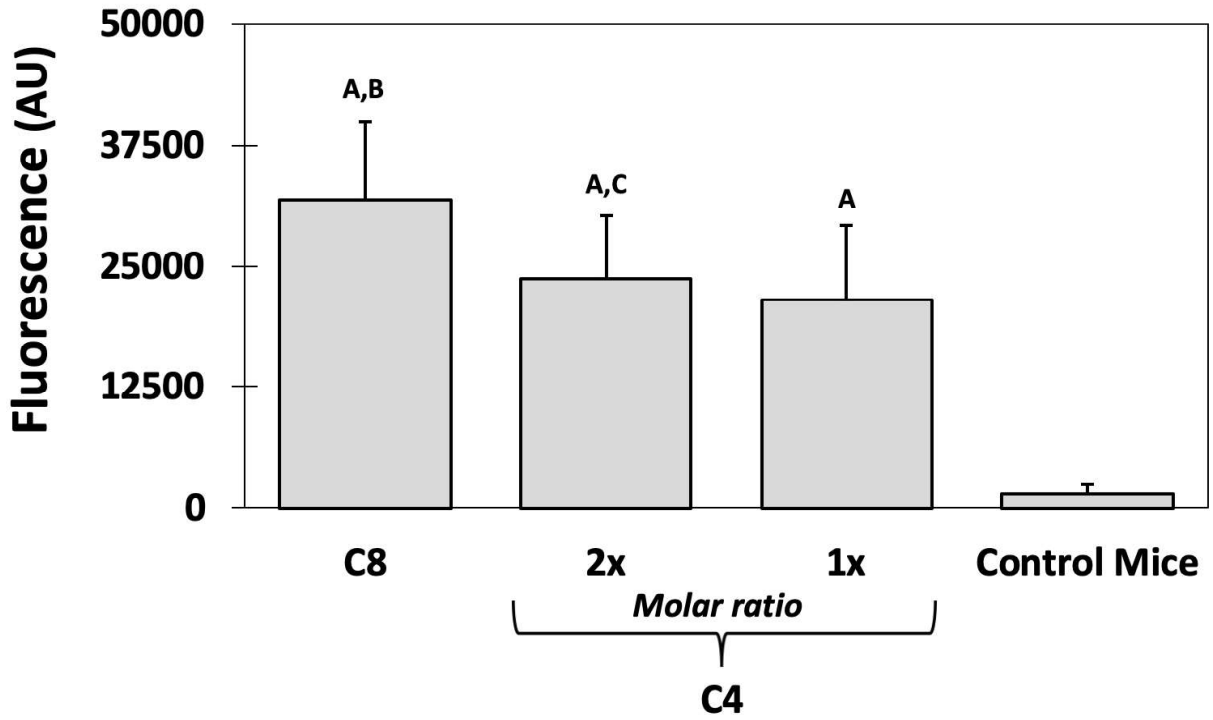

Figure 10: Cell recognition analysis for specific anti-MUC1 antibodies tested on MCF7 cells of calix[8], calix[4]. Data points represent the mean value from a group of five animals. A $p < 0.05$ compared with control; B $p > 0.05$ compared with 4 (2x and 1x); C $p > 0.05$ compared with calix[4] 1× and control. Adapted, with permission, from Spadaro *et al.*[10] (Geraci, C.; Consoli, G. M.; Granata, G.; Galante, E.; Palmigiano, A.; Pappalardo, M.; Di Puma, S. D.; Spadaro, A., First self-adjuvant multicomponent potential vaccine candidates by tethering of four or eight MUC1 antigenic immunodominant PDTRP units on a calixarene platform: synthesis and biological evaluation. Bioconjug Chem 2013, 24, 1710-20).

Conclusion

MD calculations show very different behaviour for calix[4] and calix[8], the latter being in strong agreement with the literature data. Such different behaviour allows us to hint at how the *molecular level* is useful in explaining the difference in the biological effect based on a "fit-induced" adaptation upon binding.

Calix[4] evolves to a stable globular shape with the calixarene exposed on one side. All moieties covalently bonded into the central calix are folded on the opposite side. On the contrary, calix[8] has a very flexible structure with all the moieties exposed to the solvent and the calixarene scaffold is deeply buried inside. It is also possible to highlight some differences in the two calixarene structures that can be directly related to the rigidity of the calixarene central scaffold. The calix[4] unit maintains a rigid cone conformation, while the larger calix[8] scaffold allows the rotation and a higher degree of flexibility of the phenolic ring, thus ensuring a better arrangement of the overall structure. The different conformational behaviour reflects on the electrostatic and hydrophobic maps of calix[4] vs. calix[8]. A pattern of alternating negative and positive areas, as in the anti-MUC-1 antibody which is present in the calix[8] surface in respect to that of calix[4] was detected. The PDTRP chains as in calix[8] show a conformation that better fits the binding site in terms of 3D shape, which might justify its better affinity to SM3 in respect to calix[4] as the consequence of a better complementarity. The data outlined in this research could be useful to design new vaccine constructs based on the PDTRP immunodominant MUC1 peptide sequence.

Workflow for modelling of Calix

The workflow of the *in silico* approach to study the interactions of calix[4] and calix[8] with MUC1 is reported in Figure 11

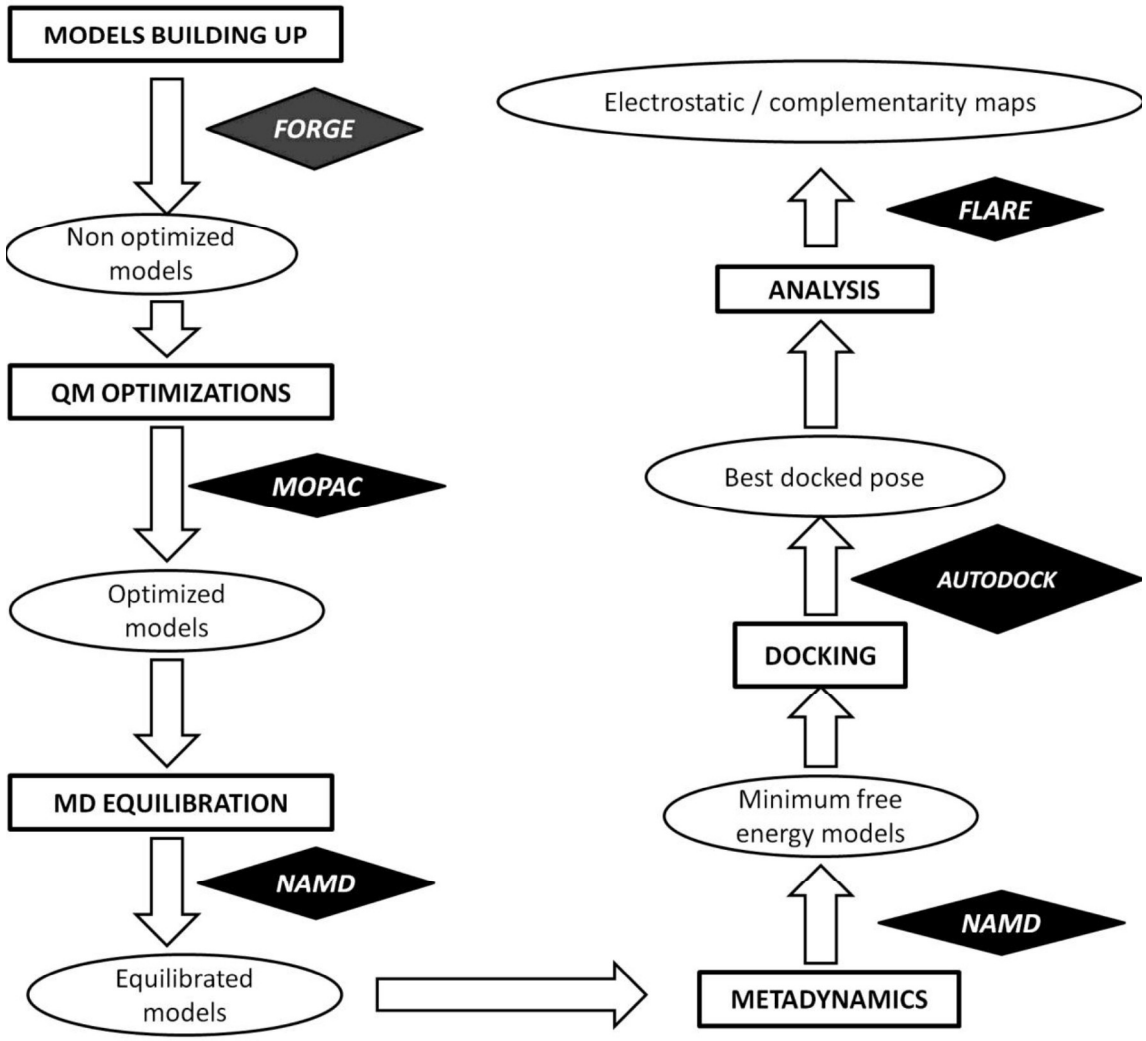

Figure 11: Molecules from previous steps (ovals), approach adopted (rectangles), used software (diamond shape).

The all-atom Calix model was built using the *Molecule Editor* as in the software Forge ver.10.4.2[18], namely one calix[4] and two calix[8] in *full cone* and *partial cone* conformations. All models were studied by the same protocol (Figure 11). Preliminary geometry optimizations of the calixarenic structures were performed with the MOPAC 2016 software[22] using the PM6 semiempirical method.[23] This approach allowed us to reduce computational time and resources and to obtain geometries that are in excellent agreement with those obtained by non-empirical approaches. The

MOPAC 2016 version is well suited for the computational studies of large molecules. The potential maps and the volumetric data sets were generated through the Cubegen utility of Gaussian09[24, 25] and imported in VMD[26].

The obtained systems were minimized for 10,000 steps using the conjugate gradient algorithm, followed by gradual heating from 0 to 310 K in 30 ps, and then maintained at a constant pressure of 1 bar for all other MD simulations. The simulation was performed using periodic boundary conditions with a time step of 2 fs and a cut-off for non-bonding interactions from 10 Å down to 12 Å.

The extended Electron Distribution (XED) [27] force field as implemented in the software Flare 2.0.1 and 3.0[18, 19] was used to generate the molecular fields on the final output MD files.

CALIX equilibration

All Molecular Dynamics simulations were carried out using the NAMD7[28, 29] software and the CHARMM27 force field.[30-33] In order to fully explore the conformational space in a reasonable time for both the calix[4] and calix[8] structures an implicit water model was used: the well-known Generalized Born Implicit Solvent Model.[34] The final box was large enough to comprise all of the atoms over the entire simulation. The size of the system was 30 Å x 30 Å x 30 Å, with a cubic shape. The cut-off values for non-bonded interactions (Coulomb and Van der Waals forces) and for the switching function were set to 9 Å, respectively. The SHAKE[35] algorithm was adopted, and long-range interactions were computed by the Particle Edwald Mesh method.[29] The time-step was fixed at 2 ps. Equilibration time was fixed at 3 ns. As Potential Energy and RMSD (Root Mean Square Deviation) became stable, the additional 100 ns of simulations were set. Each compound was considered with a total of 103 ns of simulation.

The values of the fluctuations of the backbone (RMSD) were calculated using the following equation:

$$RMSD = \sqrt{\frac{\sum_{a=1}^{Na}(\vec{r_a}(t_j) - \vec{r}_a)^2}{N_a}}$$

where Na is the number of atoms whose position must be compared, Nt is the time interval over which to compare, $\vec{r_a}(tj)$ is the position of the atom at time tj and $\vec{r_a}$ is the average position of the atom to which a is compared, which is defined as follows

$$\langle \vec{r}_a \rangle = \frac{q}{N_t} = \sum_{j=1}^{N_c} \vec{r_a}(t_j)$$

Metadynamics

After a MD equilibration of about 100 ns, metadynamics[10, 36, 37] was applied to achieve an optimal structure of calix[4] and calix[8].

It is well known that the application of metadynamics implies that an external history-dependent potential is built in the space of a few selected degrees of freedom, generally called collective variables (CVs). The choice of CV is a key step to achieve good results. Some variables were selected to highlight different behaviors in calix[4] and calix[8]. Our data indicate that the most sensitive variables are dihedral angles, as reported in Figure 2.

For the calculation, the *Metadynamics Module* inside NAMD[38, 39] was used with the same parameters as adopted in MD.

Docking

Docking was carried out with AutoDock 4.2.[40] The Lamarckian evolutionary algorithm was adopted; all parameters were kept default except for the number of genetic algorithm (GA) runs. These were set to 2500 to enhance the sampling. Atomic partial charges have been kept from our

preliminary QM calculations. The structure of the receptors was always kept rigid, whereas the structure of the calix was set partially flexible by providing freedom to some appropriately selected dihedral angles. Spacing of the box was set to 0.375 Å and its size was set to 67.00 Å in Tyr 32, Trp96, Asn31, Pro56, Val95, and Tyr102.

Complementarity Electrostatic Maps and Electrostatic maps

Positive (blue) and negative (red) protein interaction potentials were calculated for the best pose obtained from docking of calix[4] and calix[8] into tumor-specific antibody SM3 (Figure 5) by the software Flare v. 2.0.1 and 3.0[18, 19] and displayed as iso-surfaces for both the tumor-specific antibody SM3 complex with its peptide epitope (pdb code: 1sm3) and for all the calixarenes to gain insights about the binding of calix[4] and calix[8] with anti-MUC1 antibody.

Electrostatic complementarity (EC) evidences areas where protein-ligand electrostatics are favorable (green) and where electrostatics are not (red). Output for EC includes a score ranging from 1 (perfect complementarity) to -1 (strong clash).

Biological Assays

Five- to eight-week-old female Balb/c mice (Charles River, Calco, Italy) were used. Three groups of six mice were immunized twice a week at 1-week intervals by intraperitoneal injections of 0.030 μM/mouse of calix[8] (220 μg), 0.030 and 0,060 μM/mouse (125 μg and 250 μg) of calix[4]. One additional group was used as control. After 21 days from the first immunization, sera were collected and stored at −80 °C until ELISA assay. Total IgG antibodies specific to PDTRP antigen in sera were detected as previously reported and quantified by end-point dilution ELISA assay on samples pooled for each group. End-point titers were defined as the highest serum dilution that resulted in an absorbance value two times greater than that of non-immune control mouse serum with a cutoff value of 0.05. The capacity of the mouse sera to recognize native MUC1 antigen present on cancer

cells was tested as previously reported on sera obtained from the immunogenicity trials on MUC1-expressing MCF7.

Acknowledgments

The authors would like to thank Cresset (New Cambridge House, Bassingbourn Road, Litlington, Cambridgeshire, SG8 0SS, United Kingdom) for providing technical support. In particular, Dr. Giovanna Tedesco is gratefully acknowledged for very helpful discussion and suggestions. The authors gratefully acknowledge the computing time granted on the High Performance Computing (HPC) Stallo at the UiT-The Arctic University of Norway-University of Norway (http://docs.notur.no/uit). Prof. Gloria Uccello Barretta (Department of Chemistry and Industrial Chemistry, University of Pisa, Italy) and her collaborators (Dr. Federica Balzano and Dr. Andrea Cesari) are gratefully acknowledged for their helpful discussion.

References:

1. Yang, Y., Cancer immunotherapy: harnessing the immune system to battle cancer. *J Clin Invest* **2015**, 125, 3335-7.
2. Richardson, J. P.; D., M. Mucin-Based Vaccines. In *Glycoscience*, Fraiser-Reid, B., Tatsuta, K., and Thiem, J.,, Ed.; Springer-Verlag: Germany, 2008; Chapter 12.8, pp 2645-2698.
3. McCune, J. S., Immunotherapy to Treat Cancer. *Clin Pharmacol Ther* **2016**, 100, 198-203.
4. Miles, D. W.; Taylor-Papadimitriou, J., Therapeutic aspects of polymorphic epithelial mucin in adenocarcinoma. *Pharmacol Ther* **1999**, 82, 97-106.
5. Kimura, T.; Finn, O. J., MUC1 immunotherapy is here to stay. *Expert Opin Biol Ther* **2013**, 13, 35-49.

6. Pillai, K.; Pourgholami, M. H.; Chua, T. C.; Morris, D. L., MUC1 as a potential target in anticancer therapies. *Am J Clin Oncol* **2015**, 38, 108-18.
7. Martínez-Sáez, N.; Peregrina, J. M.; Corzana, F., Principles of mucin structure: implications for the rational design of cancer vaccines derived from MUC1-glycopeptides. *Chem Soc Rev* **2017**, 46, 7154-7175.
8. Wilson, R. M.; Danishefsky, S. J., A vision for vaccines built from fully synthetic tumor-associated antigens: from the laboratory to the clinic. *J Am Chem Soc* **2013**, 135, 14462-72.
9. Grinstead, J. S.; Schuman, J. T.; Campbell, A. P., Epitope mapping of antigenic MUC1 peptides to breast cancer antibody fragment B27.29: a heteronuclear NMR study. *Biochemistry* **2003**, 42, 14293-305.
10. Geraci, C.; Consoli, G. M.; Granata, G.; Galante, E.; Palmigiano, A.; Pappalardo, M.; Di Puma, S. D.; Spadaro, A., First self-adjuvant multicomponent potential vaccine candidates by tethering of four or eight MUC1 antigenic immunodominant PDTRP units on a calixarene platform: synthesis and biological evaluation. *Bioconjug Chem* **2013**, 24, 1710-20.
11. Geraci, C.; Consoli, G. M.; Galante, E.; Bousquet, E.; Pappalardo, M.; Spadaro, A., Calix[4]arene decorated with four Tn antigen glycomimetic units and P3CS immunoadjuvant: synthesis, characterization, and anticancer immunological evaluation. *Bioconjug Chem* **2008**, 19, 751-8.
12. Müller, C.; Despras, G.; Lindhorst, T. K., Organizing multivalency in carbohydrate recognition. *Chem Soc Rev* **2016**, 45, 3275-302.
13. Kiessling, L. L.; Young, T.; Gruber, T. D.; Mortell, K. H. Multivalency in Protein–Carbohydrate Recognition. In *Glycoscience: Chemistry and Chemical Biology*, Fraser-Reid, B. O.; Tatsuta, K.; Thiem, J., Eds.; Springer Berlin Heidelberg: Berlin, Heidelberg, 2008, pp 2483-2523.
14. Singharoy, A.; Polavarapu, A.; Joshi, H.; Baik, M. H.; Ortoleva, P., Epitope fluctuations in the human papillomavirus are under dynamic allosteric control: a computational evaluation of a new vaccine design strategy. *J Am Chem Soc* **2013**, 135, 18458-68.
15. Liu, Y.; Singharoy, A.; Mayne, C. G.; Sengupta, A.; Raghavachari, K.; Schulten, K.; Flood, A. H., Flexibility Coexists with Shape-Persistence in Cyanostar Macrocycles. *J Am Chem Soc* **2016**, 138, 4843-4851.
16. Sgarlata, C.; Brancatelli, G.; Fortuna, G.; Sciotto, D.; Silvano, G.; Bonaccorso, C., 3D network structures based on pyridyl-calix 4 arene metal complexes. *ChemPlusChem* **2017**, 82.
17. Escudero, C.; D'Urso, A.; Lauceri, R.; Bonaccorso, C.; Sciotto, D.; Di Bella, S.; Zoubir, M.; Crusats, J.; Ribo, J., M. ; Purrello, R., Hierarchical dependence of porphyrin self-aggregation: Controlling and exploiting the complexity. *Journal of Porphyrins and Phthalocyanines* **2010**, 14, 708-712.
18. Cheeseright, T.; Mackey, M.; Rose, S.; Vinter, A., Molecular field extrema as descriptors of biological activity: definition and validation. *J Chem Inf Model* **2006**, 46, 665-76.
19. Bauer, M. R.; Mackey, M. D., Electrostatic Complementarity as a Fast and Effective Tool to Optimize Binding and Selectivity of Protein-Ligand Complexes. *J Med Chem* **2019**, 62, 3036-3050.
20. Tzlil, S.; Murray, D.; Ben-Shaul, A., The "electrostatic-switch" mechanism: Monte Carlo study of MARCKS-membrane interaction. *Biophys J* **2008**, 95, 1745-57.
21. Bauer, M. R.; Mackey, M. D., Electrostatic complementarity as a fast and effective tool to optimize binding and selectivity of protein-ligand complexes. *J Med Chem* **2019**.
22. Stewart, J. J. P. MOPAC2016.
23. Stewart, J. J., Optimization of parameters for semiempirical methods V: modification of NDDO approximations and application to 70 elements. *J Mol Model* **2007**, 13, 1173-213.
24. Stewart, J. J., MOPAC: a semiempirical molecular orbital program. *J Comput Aided Mol Des* **1990**, 4, 1-105.
25. Tamura, T., [Introduction of MOPAC simulation for experimental biochemists]. *Seikagaku. The Journal of Japanese Biochemical Society* **2010**, 82, 863-7.
26. Humphrey, W.; Dalke, A.; Schulten, K., VMD: Visual molecular dynamics. *J Mol Graph Model* **1996**, 14, 33-38.
27. Vinter, J. G., Extended electron distributions applied to the molecular mechanics of some intermolecular interactions. *J Comput Aided Mol Des* **1994**, 8, 653-68.
28. Nelson, M. T.; Humphrey, W.; Gursoy, A.; Dalke, A.; Kale, L. V.; Skeel, R. D.; Schulten, K., NAMD: A parallel, object oriented molecular dynamics program. *Int J Supercomput Ap* **1996**, 10, 251-268.

29. Phillips, J. C.; Braun, R.; Wang, W.; Gumbart, J.; Tajkhorshid, E.; Villa, E.; Chipot, C.; Skeel, R. D.; Kale, L.; Schulten, K., Scalable molecular dynamics with NAMD. *J Comput Chem* **2005**, 26, 1781-1802.
30. Pavelites, J. J.; Gao, J. L.; Bash, P. A.; Mackerell, A. D., A molecular mechanics force field for NAD(+), NADH, and the pyrophosphate groups of nucleotides. *J Comput Chem* **1997**, 18, 221-239.
31. MacKerell, A. D., Developments in the CHARMM all-atom empirical energy function for biological molecules. *Abstr Pap Am Chem S* **1998**, 216, U696-U696.
32. MacKerell, A. D.; Bashford, D.; Bellott, M.; Dunbrack, R. L.; Evanseck, J. D.; Field, M. J.; Fischer, S.; Gao, J.; Guo, H.; Ha, S.; Joseph-McCarthy, D.; Kuchnir, L.; Kuczera, K.; Lau, F. T. K.; Mattos, C.; Michnick, S.; Ngo, T.; Nguyen, D. T.; Prodhom, B.; Reiher, W. E.; Roux, B.; Schlenkrich, M.; Smith, J. C.; Stote, R.; Straub, J.; Watanabe, M.; Wiorkiewicz-Kuczera, J.; Yin, D.; Karplus, M., All-atom empirical potential for molecular modeling and dynamics studies of proteins. *J Phys Chem B* **1998**, 102, 3586-3616.
33. Yin, D. X.; Mackerell, A. D., Combined ab initio empirical approach for optimization of Lennard-Jones parameters. *J Comput Chem* **1998**, 19, 334-348.
34. Bashford, D.; Case, D. A., Generalized born models of macromolecular solvation effects. *Annu Rev Phys Chem* **2000**, 51, 129-52.
35. Ryckaert, J.-P.; Ciccotti, G.; Berendsen, H. J. C., Numerical integration of the cartesian equations of motion of a system with constraints: molecular dynamics of n-alkanes. *Journal of Computational Physics* **1977**, 23, 327-341.
36. Chu, Y.; Xia, M.; Lin, Y.; Li, A.; Wang, Y.; Liu, R.; Xiong, S., Th2-dominated antitumor immunity induced by DNA immunization with the genes coding for a basal core peptide PDTRP and GM-CSF. *Cancer Gene Ther* **2006**, 13, 510-9.
37. Ingale, S.; Wolfert, M. A.; Buskas, T.; Boons, G. J., Increasing the antigenicity of synthetic tumor-associated carbohydrate antigens by targeting Toll-like receptors. *Chembiochem* **2009**, 10, 455-63.
38. Barducci, A.; Bussi, G.; Parrinello, M., Well-tempered metadynamics: a smoothly converging and tunable free-energy method. *Physical review letters* **2008**, 100, 020603.
39. Laio, A.; Parrinello, M., Escaping free-energy minima. *Proceedings of the National Academy of Sciences of the United States of America* **2002**, 99, 12562-6.
40. Morris, G. M.; Huey, R.; Lindstrom, W.; Sanner, M. F.; Belew, R. K.; Goodsell, D. S.; Olson, A. J., AutoDock4 and AutoDockTools4: Automated docking with selective receptor flexibility. *J Comput Chem* **2009**, 30, 2785-91.